Downloaded from orbit.dtu.dk on: Apr 19, 2024

DTU Library

Exploring the Intrinsic Point Defects in Cesium Copper Halides

Lan, Zhenyun; Meng, Jie; Zheng, Kaibo; Castelli, Ivano Eligio

Published in:
Journal of Physical Chemistry C

Link to article, DOI:
10.1021/acs.jpcc.0c11216

Publication date:
2021

Document Version
Peer reviewed version

Link back to DTU Orbit

Citation (APA):
Lan, Z., Meng, J., Zheng, K., & Castelli, I. E. (2021). Exploring the Intrinsic Point Defects in Cesium Copper Halides. *Journal of Physical Chemistry C*, *125*(2), 1592-1598. https://doi.org/10.1021/acs.jpcc.0c11216

General rights
Copyright and moral rights for the publications made accessible in the public portal are retained by the authors and/or other copyright owners and it is a condition of accessing publications that users recognise and abide by the legal requirements associated with these rights.

- Users may download and print one copy of any publication from the public portal for the purpose of private study or research.
- You may not further distribute the material or use it for any profit-making activity or commercial gain
- You may freely distribute the URL identifying the publication in the public portal

If you believe that this document breaches copyright please contact us providing details, and we will remove access to the work immediately and investigate your claim.

Exploring the Intrinsic Point Defects in Cesium Copper Halides

*Zhenyun Lan,[a, 1, *] Jie Meng,[b,1] Kaibo Zheng,[b,c] and Ivano E. Castelli [a,*]*

[a]*Department of Energy Conversion and Storage, Technical University of Denmark, Anker Engelundsvej 411, DK-2800 Kgs. Lyngby, Denmark*

[b]*Department of Chemistry, Technical University of Denmark, DK-2800 Kgs. Lyngby, Denmark*

[c]*ChemicalPhysics and NanoLund, Lund University, 22100 Lund, Sweden*

E-mail address: zhenlan@dtu.dk (ZL); ivca@dtu.dk (IEC)

[1]These authors contributed equally to this work

Abstract

Cesium copper halides $Cs_3Cu_2X_5$ (X=Cl, Br and I) have attracted much attention for optoelectronic applications because of their self-trap excitons (STE) and high photoluminescence quantum yield (PLQY). Intrinsic point defects play a critical role in the optoelectronic performance of these materials by affecting fundamental properties, such as carrier mobility, lifetime, and recombination rate. In this work, we have calculated, by means of quantum mechanical calculations, formation energies and transition levels of all possible intrinsic point defects in $Cs_3Cu_2X_5$. We have found that only X_i and X_{Cs} defects show simultaneously, deep transition energy levels and negative formation energies. Interestingly, the dominant defect under halide-rich growth condition exhibits much higher concentration than that under halide-poor condition. Thus avoiding the halide-rich condition could help in reducing the defect concentration.

Introduction

Lead-free metal halide materials have attracted considerable interest to replace lead halide perovskites ($CsPbX_3$, X=Cl, Br and I) due to their low-toxicity, high-stability and optimal optical properties.[1,2] Among them, inorganic cesium copper halides $Cs_3Cu_2X_5$ (X=Cl, Br and I) with superior luminescence properties (near-unity photoluminescence quantum yield (PLQY), have been regarded as promising candidates for their potential applications in photoluminescence, LED, photodetector and so on.[3–5] The superior PLQY properties of $Cs_3Cu_2X_5$ materials compared with other lead-free materials, such as $Cs_3Bi_2X_9$, $CsGeX_3$, and Cs_2AgBiX_3,[6] are generated by their stronger quantum confinement, site isolation, zero-dimensional structure at the molecular level (0D), and correspondingly strong self-trap excitons (STE) emission, and large exciton binding energy. These outstanding factors make $Cs_3Cu_2X_5$ ideal candidates for optoelectronic devices.[7–9]

Any deviation from periodic crystal lattice would result in crystal imperfections, namely defects, which might form localized electronic states (defect energy levels)[10] that, if are located inside the band gap region, will trap photo-excited charge carriers and limit their mobility, with serious repercussion on the efficiency of the device.[11] From reported experimental results, the PLQY varies under different synthesis conditions as defects formation will primarly rely on the growth environment.[3,4,12] Therefore, understanding the role of defects, and particularly of intrinsic point defects, is thus of pivotal importance. Although the synthesis and superior properties of low-dimensional copper halides $Cs_3Cu_2X_5$ have been recently reported,[4,8,13,14] a comprehensive theoretical investigation of the properties of the defects, from their formation

energies under different growth conditions to their charge-transition levels, is still missing.[15,16] Here, by studying defects properties with atomic-scale simulations, we aim to provide a guideline to reduce the defects concentration and ultimately synthesize high-quality $Cs_3Cu_2X_5$ with high PLQY. We perform Density Functional Theory (DFT) calculations to estimate the formation energies and transition levels of all possible intrinsic point defects in $Cs_3Cu_2X_5$. We find that despite their differences as pure elements, the three halides form compounds with similar properties in terms of electronic structures, defect formation energies and charge transition levels. Among all the possible point defects considered, Cu_i, X_i and X_{Cs} are easier to form, with negative formation energies and higher defect concentration. Only X_i and X_{Cs} defects show, simultaneously, deep transition energy levels in the band gap region and negative formation energies, which is energetically favorable to trap the photo-generated charge carrier from the band edge excited states. Therefore, these two kinds of defects should be avoided during synthesis. By calculation of formation energy under different growth condition, we find that the defects formation energies depend on the synthesis conditions: under halide-poor growth condition, the dominant defects (X_i) exhibit much higher formation energies than under halide-rich conditions, which could thus help to reduce the defects concentration and avoid the formation of trap states.

Method

DFT calculations were performed with the VASP package.[17] The generalized gradient approximation (GGA)[18] in the description from Perdew−Burke−Ernzerhof (PBE) was used as exchange-correlation functional and the projector augmented wave (PAW)[19] potentials for Cs,

Cu, Cl, Br and I atoms, with a 500 eV plane-wave cutoff. We used a 4 x 4 x 3 Γ-centered Monkhorst–Pack k-point mesh for the unit cell composed of 40 atoms, while for the 2 x 2 x 2 supercell, necessary to avoid the interaction between defects, we used a single k-point (Γ).[20] The possible intrinsic points defects considered are vacancies (V_{Cs}, V_{Cu}, V_X), interstitial (Cs_i, Cu_i, X_i) and antisites (Cs_X, Cs_{Cu}, Cu_X, Cu_{Cs}, X_{Cs}, X_{Cu}) as shown in **Figure S1-3**. The crystal structures and internal atomic positions were fully relaxed until the forces were below 0.02 eV/Å. The exciton binding energies were calculated using the Wannier-Mott (WM) model: $E_b = R_\infty \mu/(m_0 \varepsilon^2)$, where the reduced effective mass of the e-h pair, μ, is equal to $(m_e^{*-1}+m_h^{*-1})^{-1}$, R_∞ the Rydberg constants. ε is the dielectric constant, calculated using Density functional perturbation theory (DFPT)[21] and both average static dielectric constant ε_s and average macroscopic dielectric constant ε_0 calculated from the frequency-dependent dielectric functions were considered.[22] The formation energy of a defect or impurity X in charge state q is defined as:

$$E_f(X_q) = E_{tot}(X_q) - E_{tot}(\text{host}) + \sum_i (n_i + \mu_i) + q(E_v + \varepsilon_f + \Delta V) \quad \ldots\ldots\ldots\ldots\ldots\ldots\ldots\ldots (1)$$

where $E_{tot}(X_q)$ is the total energy of a supercell with defect X with charge q in the cell. E_{tot} (host) is the total energy of the supercell without any defects. n_i indicates the number of atom i that has been added to (or removed from) the supercell when the defect is created. μ_i is the chemical potential of corresponding atom i. E_v is the valence band maximum (VBM) of the perfect supercell. ε_f is the fermi lever referenced to the E_v. The correction term ΔV is the shift of the VBM between different defects charge states and the defect-free supercell.[23] It can be obtained by calculating the shift of the 1s core level of a Cs atom in the defect-free and defect supercell.[15] The defect charge-transition energy level $\varepsilon(q_1/q_2)$ is the Fermi energy at which the formation

energy of a defect with charge q_1 is equal to the one with charge q_2:[24]

$$\varepsilon(q_1/q_2) = [E_{q_1} + E_{q_2} + q_1(E_V+\Delta V_1) - q_2(E_V+\Delta V_2)]/(q_2-q_1) \quad \ldots\ldots(2)$$

where q_1 and q_2 are the initial and final charge states. ΔV_1 (ΔV_2) is the shift of VBM between q_1 charge defects (q_2 charge states) and the defect-free supercell. We are aware that the band gap calculated with at the PBE level is underestimated and this might affect the values of the band gap. However, as it has been shown previously that GGA and hybrid exchange-correlation functionals predict similar defect Kohn–Sham levels.[25] More in details, the charge transition levels of dominant defects calculated at the HSE hybrid functional with Spin Orbit Coupling (SOC) correction and at the PBE level, without SOC correction, has been shown to be in good agreement. Therefore, we consider that the choice of using the PBE functional to calculate the defect formation energies and charge-state transition levels is reasonable. All the structures and outputs of the calculations are stored and freely available in the DTU DATA repository (DOI: 10.11583/DTU.12981887).

Result and discussion

The crystal structures of the materials investigated here are shown in **Figure 1**. These crystals have orthorhombic symmetry (*Pnma* space group) and their lattice parameters increase following the trend I > Br > Cl (the experimental and theoretical values are listed in Supporting Information, Table S1).[26,27] Typically, in these structures, $[Cu_2X_5]^{3-}$ clusters are isolated from the Cs^+ cations, forming a unique 0D structure at the molecular level and they exhibit two types of Cu^+ sites, a tetrahedral site (for X=Br and I) and a trigonal site (for X=Cl, Br and I). Because of the unique 0D structure, these materials show remarkably large exciton binding energy, high

PLQYs, and increased stability.[12]

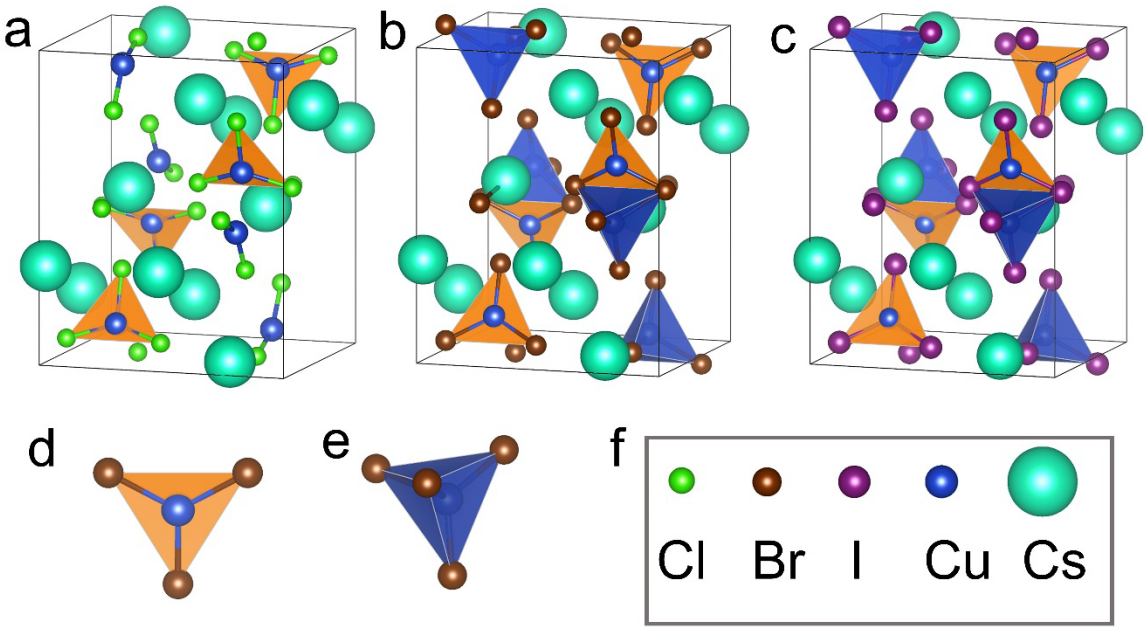

Figure 1. Crystal structure of $Cs_3Cu_2X_5$ for X=Cl (a), Br (b), and I (c). (d) The three- and (e) four-coordinated Cu ions are shown in the orange and blue, respectively. (f) Cs and Cu are indicated with cyan and blue spheres, respectively. The halides, Cl, Br, and I are shown with green, brown and purple spheres.

Band structures (**Figure 2a-c**) and the projected density of states (PDOS, **Figure 2d-f**) are calculated to investigate the electronic properties. Both conduction band minimum (CBM) and valence band maximum (VBM) are located at the Γ point, which indicates that $Cs_3Cu_2X_5$ have direct band gaps. The calculated band gaps of $Cs_3Cu_2Cl_5$, $Cs_3Cu_2Br_5$ and $Cs_3Cu_2I_5$ have similar values (2.35 eV, 2.10 eV and 2.33 eV, respectively), which is consistent with previously reported results at the PBE level.[4] For better accuracy, we have calculated the band gap using the HSE06 hybrid functional and adding the SOC correction.[28] The gaps now follow the trend expected by the change in electronegativity of the anions (Cl > Br > I) and equal to 3.66, 3.40

and 3.29 eV, respectively as shown in **Table 1**. We would like to point out that, as indicated in the method section and shown previously in the literature, [25] the results reported here regarding the defects calculations performed at the PBE level are still valid. The conduction band (CB) is predominantly composed of Cu 4s.[29] The valence band (VB) is, instead, mainly formed by Cu 3d orbital hybridized with the halide p orbitals (3p, 4p, 5p for Cl, Br and I, respectively). The Cs^+ ions do not contribute to either the CBM or the VBM, acting purely as an electron donor, which can be evinced by looking at the $Cs_3Cu_2X_5$ structures (**Figure 1**).[30]

To better explore the optical properties, the effective mass and exciton binding energy were calculated and reported in **Table 2**. The calculated exciton binding energies for $Cs_3Cu_2X_5$ ranges from 261 to 675 meV (275 to 723 meV) are in the same magnitude order as the reported results.[12,16] Because excitons binding energies are considerably higher than the thermal energy k_BT at room temperature (~26 meV), excitons are the majority of the photo-excited species, which indicates that the robust photoluminescence is originated from exciton recombination. Among all $Cs_3Cu_2X_5$ compounds, $Cs_3Cu_2Cl_5$ shows the largest exciton binding energy, consistent with its superior PLQY properties (near one-unity).[7] This suggests that improved efficiency could be achieved by simultaneously increasing the exciton binding energies and decreasing defect concentration. We note that the exciton binding energies of $Cs_3Cu_2X_5$ materials are much larger than for conventional cesium lead perovskite halides (the estimated exciton binding energies for $CsPbCl_3$, $CsPbBr_3$, and $CsPbI_3$ QDs are 75, 40, 20 meV, respectively).[31] This indicates that excitons play a more critical role in the photophysics process and photoelectric properties for $Cs_3Cu_2X_5$ compared with $CsPbX_3$.

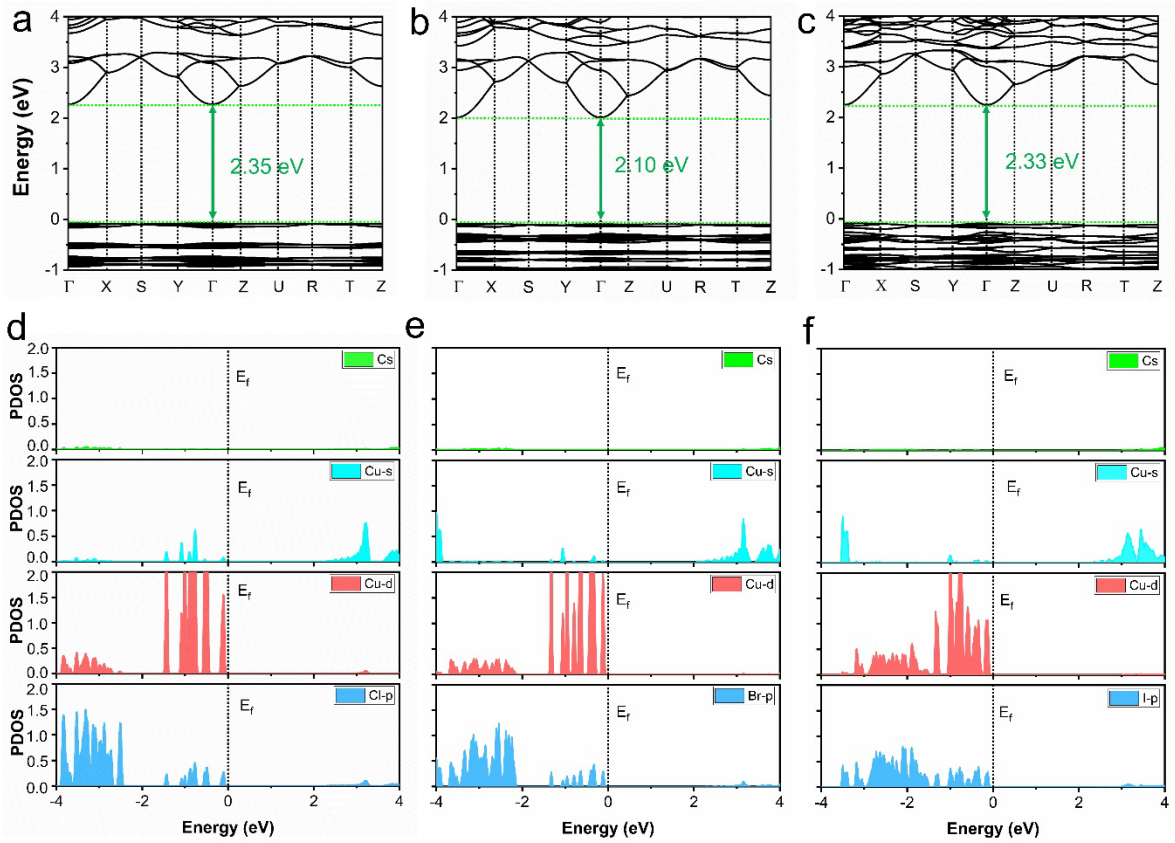

Figure 2. Band structure and projected density of states (PDOS) of $Cs_3Cu_2X_5$ (X=Cl, Br, I). (a, d) $Cs_3Cu_2Cl_5$, (b, e). $Cs_3Cu_2Br_5$ and (c, f) $Cs_3Cu_2I_5$. The Fermi energy (E_F) was set to 0 eV. The PDOS values are normalized by atoms orbital numbers.

Table 1. Calculated band gap of $Cs_3Cu_2X_5$ (X=Cl Br and I) using the HSE hybrid functional with and without SOC correction

	$Cs_3Cu_2Cl_5$ (eV)	$Cs_3Cu_2Br_5$ (eV)	$Cs_3Cu_2I_5$ (eV)
HSE without SOC	3.91	3.65	3.66
HSE with SOC	3.66	3.40	3.29

Table 2. Calculated electron effective mass (m_e^*), hole effective mass (m_h^*), average static dielectric constant (ε_s), average macroscopic dielectric constant (ε_0) and exciton binding energies (E_b (meV))

	m_e^*/m_0 (Y-Γ)	m_h^*/m_0 (Γ-Z)	ε_s	ε_0	E_b (ε_s)	E_b (ε_0)
$Cs_3Cu_2Cl_5$	0.503	12.346	3.121	3.015	675	723
$Cs_3Cu_2Br_5$	0.381	11.338	3.435	3.365	425	454
$Cs_3Cu_2I_5$	0.321	3.230	2.901	3.852	261	275

Defects in the materials will affect the photophysical properties.[32] According to equation (1), the formation energies for different defects in neutral charge states are affected by the chemical potential of the corresponding atom,[33,34] which dependents on the synthesis conditions. In this work, the chemical potential, μ_i, is referenced to Cs metal, Cu metal, Cl_2 molecule, Br_2 molecule, or I solids. To prevent the formation of elemental solids, all μ_i should be negative ($\mu_{Cs} < 0$, $\mu_{Cu} < 0$, and $\mu_X < 0$). In addition, to avoid the phase separation into known binary and ternary compounds, the following constraints also need to be satisfied:

For $Cs_3Cu_2Cl_5$,

$\mu_{Cs} + \mu_{Cl} < \Delta H(CsCl)$……(3)

$\mu_{Cu} + 2\mu_{Cl} < \Delta H(CuCl_2)$ ……..(4)

$\mu_{Cs} + \mu_{Cu} + 3\mu_{Cl} < \Delta H(CsCuCl_3)$ ……..(5)

$\mu_{Cs} + 2\mu_{Cu} + 3\mu_{Cl} < \Delta H(CsCu_2Cl_3)$ ……...(6)

$2\mu_{Cs} + \mu_{Cu} + 4\mu_{Cl} < \Delta H(Cs_2CuCl_4)$ ……..…….(7)

For $Cs_3Cu_2Br_5$,

$\mu_{Cs} + \mu_{Br} < \Delta H(CsBr)$..……..(8)

$\mu_{Cu} + \mu_{Br} < \Delta H(CuBr)$..……..(9)

$\mu_{Cu} + 2\mu_{Br} < \Delta H(CuBr_2)$……(10)

$\mu_{Cs} + 3\mu_{Br} < \Delta H(CsBr_3)$……(12)

$\mu_{Cs} + \mu_{Cu} + 3\mu_{Br} < \Delta H(CsCuBr_3)$……(13)

$\mu_{Cs} + 2\mu_{Cu} + 3\mu_{Br} < \Delta H(CsCu_2Br_3)$……(14)

For $Cs_3Cu_2I_5$,

$\mu_{Cs} + \mu_I < \Delta H(CsI)$……....(15)

$\mu_{Cu} + \mu_I < \Delta H(CuI)$……(16)

$\mu_{Cu} + 3\mu_I < \Delta H(CuI_3)$……(17)

$\mu_{Cu} + 4\mu_I < \Delta H(CuI_4)$……(18)

where ΔH is the formation energy of the compounds and the structures are taken from the Materials Project database.[35]

Last, to form the stable $Cs_3Cu_2X_5$, the following equation should be satisfied:

$3\mu_{Cs} + 2\mu_{C\mu} + 5\mu_X = \Delta H(Cs_3Cu_2X_5)$ (X=Cl, Br and I)……(19)

Set these constraints, the chemical potential of Cs is calculated as a function of the chemical potential of Cu and X. The stability region as a function of the chemical potential of $Cs_3Cu_2X_5$ is indicated with a yellow area in **Figure 3**. The four points defining the yellow region are chosen to calculate the neutral defects formation energies, where point B represents the X rich and Cu poor condition while point D corresponds to X poor and Cu rich condition. The formation energies of these defects (vacancies, interstitials, and antisites) at these four points are listed in Tables 2-4, for Cl, Br, and I, respectively. It is interesting to note that, both under halide X-rich (B) and X-poor condition (D), the interstitials X_i have the lowest formation energies, and therefore, they are the dominant defects. To further evaluate the intrinsic defect

concentration, c_i, at room temperature (T=300 K), the Boltzmann distribution $\exp(-\Delta E_f/k_B T)$ was used, where ΔE_f is formation energy of defect, k_B is the Boltzmann constant and T is temperature.[36] Conventionally, for intrinsic defects, a larger value of c_i means higher defect concentration (the calculated values are reported in Table S5). Generally, the X_i defect concentration in the halide rich condition is much larger than that in the halide-poor condition. Hence, to avoid the formation of the dominant defects, the growth should be performed under halide-poor conditions. Meanwhile, other intrinsic defects, like Cu_i and X_{Cs}, also show negative defect formation energies regardless of halide poor/rich condition, meaning they could form spontaneously, which should also be noticed during synthesis.

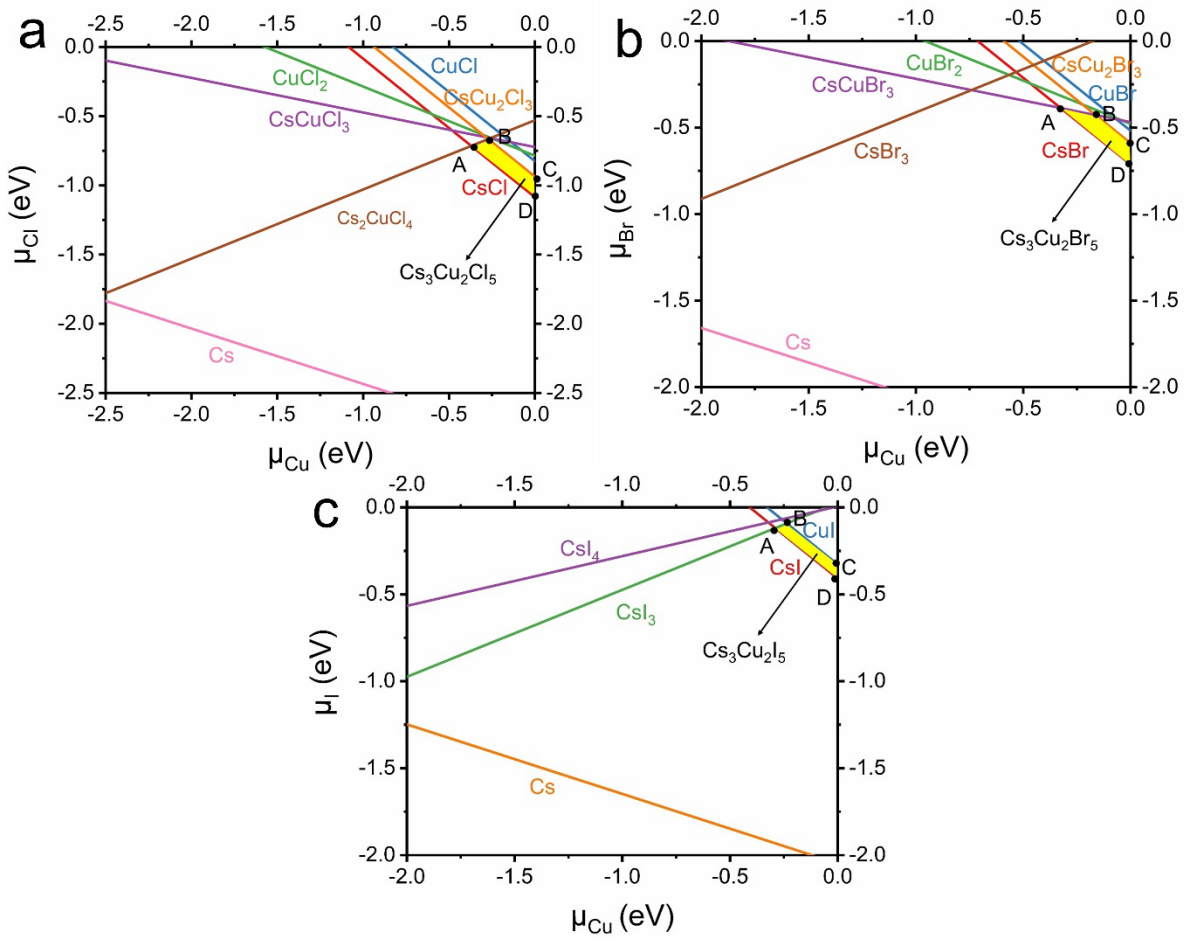

Figure 3. The calculated stability region as a function of the chemical potential of (a) $Cs_3Cu_2Cl_5$, (b) $Cs_3Cu_2Br_5$ and (c) $Cs_3Cu_2I_5$ is indicated in yellow. The positions of A, B, C and D are chosen to investigate the defect formation energy, as shown in supporting information (Table S2-4).

Table 2. Calculated formation energies (in eV) for neutral defects in $Cs_3Cu_2Cl_5$ at the four chosen points A, B, C and D from Figure 3a.

	V_{Cl}	V_{Cs}	V_{Cu}	Cs_{Cl}	Cl_{Cs}	Cl_{Cu}	Cu_{Cl}	Cs_i	Cl_i	Cu_i
A	4.603	0.492	3.207	6.011	-1.400	1.745	1.418	4.081	-1.863	-0.538
B	4.652	0.350	3.305	6.207	-1.596	1.794	1.369	4.228	-1.912	-0.636
C	4.380	0.616	3.578	5.664	-1.053	2.339	0.824	3.957	-1.640	-0.909
D	4.232	0.863	3.578	5.269	-0.658	2.487	0.676	3.710	-1.492	-0.909

Table 3. Calculated formation energies (in eV) for neutral defects in $Cs_3Cu_2Br_5$ at the four chosen points A, B, C and D from Figure 3b.

	V_{Br}	V_{Cs}	V_{Cu}	Cs_{Br}	Br_{Cs}	Br_{Cu}	Cu_{Br}	Cs_i	Br_i	Cu_i
A	4.379	0.547	3.290	6.035	-1.054	2.152	1.272	2.711	-1.551	-0.600
B	4.339	0.505	3.450	6.037	-1.056	2.355	1.069	2.753	-1.511	-0.763
C	4.176	0.669	3.615	5.710	-0.729	2.68	0.744	2.589	-1.348	-0.925
D	4.054	0.872	3.615	5.385	-0.404	2.802	0.622	2.386	-1.226	-0.925

Table 4. Calculated formation energies (in eV) for neutral defects in $Cs_3Cu_2I_5$ at the four chosen points A, B, C and D from Figure 3c.

	V_I	V_{Cs}	V_{Cu}	Cs_I	I_{Cs}	I_{Cu}	Cu_I	Cs_i	I_i	Cu_i
A	4.198	0.755	3.62	5.747	-0.325	2.506	1.092	2.791	-0.883	-0.748

B	4.224	0.675	3.68	5.853	-0.431	2.535	1.063	2.871	-0.909	-0.803
C	3.988	0.911	3.911	5.381	0.041	3.007	0.591	2.635	-0.673	-1.039
D	3.908	1.045	3.911	5.167	0.255	3.087	0.511	2.501	-0.593	-1.039

Deep transition levels might act as carrier trap states, thus induce nonradiative recombination and weaken the optoelectronic properties. Following equation 2, we have calculated the charge transition levels for different defects (**Figure 4**). Most of the calculated points defects are located in deep transition levels, which is different from $CsPbX_3$, where only a few defects are found in deep transition levels.[15,37,38] Combining the calculated formation energies of points defects in **Table 2-4** and the charge transition levels for different defects shows that only X_{Cs} and X_i with negative formation energies show deep transition energy levels. Hence, these defects are the primary trap states that should be avoided in the synthesis conditions. Independently from the halide, all $Cs_3Cu_2X_5$ structures exhibit similar phenomena for the defect formation energies and transition energy levels.

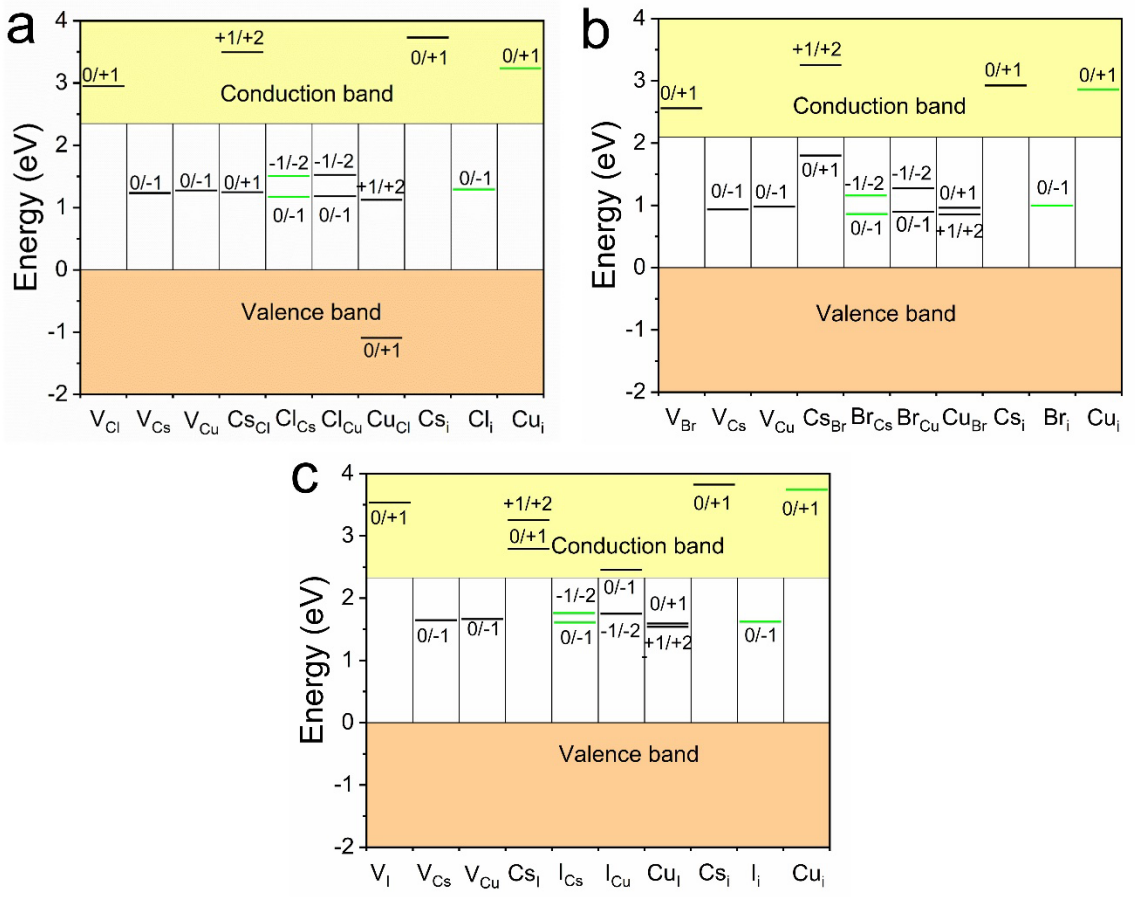

Figure 4. The charge transition level of defects for (a) $Cs_3Cu_2Cl_5$, (b). $Cs_3Cu_2Br_5$ and (c) $Cs_3Cu_2I_5$.The green lines indicate the formation energies of these neutral defects are negative. The black lines mean the formation energies of these neutral defects are positive.

Conclusion

In this work, we have studied the formation energies and charge transition levels of all possible intrinsic point defects in $Cs_3Cu_2X_5$ (X=Cl, Br, I) using DFT calculations. We find that interstitial Cu_i and X_i, and antisites X_{Cs} show negative formation energies and higher defect concentration compared to other point defects. Combining these results with the calculated charge transition levels, only X_i and X_{Cs} defects show deep transition energy levels, which would act as a trap state. Therefore, these kinds of defects should be avoided during synthesis. The

calculated formation energies indicate that halide-rich conditions will lead to high defect concentration, such as X_{Cs} and X_i. Therefore, to reduce the concentration of defects, the growth should be under moderate or halide-poor conditions. The large exciton binding energies could also help to increase the PLQY once we efficiently suppress the formation of defects. Our work can guide experiments in setting up the right conditions to synthesize materials with high-quality optoelectronic properties by reducing the defects concentrations. Starting from the results described here, the natural extension of this work is to investigate defects in a surface model, which can provide insight into the position of the defects and a closer correlation to understand the PLQY properties better.

ASSOCIATED CONTENT

Supporting Information

Lattice parameters for different sturctures, chemical potential at different points, calculated $\exp(-\Delta E_f/k_BT)$, calculated band gap of $Cs_3Cu_2X_5$ (X=Cl Br and I), crystal structure of Cs_3Cu_2X (X=Cl, Br or I) and schematic picture of interstitials defects.

Corresponding Author

zhenlan@dtu.dk (ZL); ivca@dtu.dk (IEC)

ORCID

Jie Meng: 0000-0002-3813-5221

Zhenyun Lan: 0000-0001-7943-5936

Kaibo Zheng: 0000-0002-7236-1070

Ivano E. Castelli 0000-0001-5880-5045

Notes

The authors declare no competing financial interest.

Acknowledge

Z.L. and J.M. acknowledge support from the China Scholarship Council (CSC). K.Z. thanks the support from Independent Research Fund Denmark-Sapere Aude starting grant (No. 7026-00037A) and Swedish Research Council VR starting grant (No. 2017-05337), I.E.C. wishes to acknowledge the support from the Department of Energy Conversion and Storage, Technical University of Denmark, through the Special Competence Initiative "Autonomous Materials Discovery (http://www.aimade.org/)".

References

(1) Xiao, Z.; Song, Z.; Yan, Y. From Lead Halide Perovskites to Lead-Free Metal Halide Perovskites and Perovskite Derivatives. *Adv. Mater.* **2019**, *31*, 1803792.

(2) Yang, S.; Fu, W.; Zhang, Z.; Chen, H.; Li, C.-Z. Recent Advances in Perovskite Solar Cells: Efficiency, Stability and Lead-Free Perovskite. *J. Mater. Chem. A* **2017**, *5*, 11462–11482.

(3) Sebastia-Luna, P.; Navarro-Alapont, J.; Sessolo, M.; Palazon, F.; Bolink, H. J. Solvent-Free Synthesis and Thin-Film Deposition of Cesium Copper Halides with Bright Blue Photoluminescence. *Chem. Mater.* **2019**, *31*, 10205–10210.

(4) Luo, Z.; Li, Q.; Zhang, L.; Wu, X.; Tan, L.; Zou, C.; Liu, Y.; Quan, Z. 0D Cs 3 Cu 2 X 5 (X = I, Br, and Cl) Nanocrystals: Colloidal Syntheses and Optical Properties. *Small* **2020**, *16*, 1905226.

(5) Jun, T.; Sim, K.; Iimura, S.; Sasase, M.; Kamioka, H.; Kim, J.; Hosono, H. 81-5: Late-News Paper: Pb-free Blue-emitting 0D Cs 3 Cu 2 I 5 with High PLQY of ~90%. *SID Symp. Dig. Tech. Pap.* **2019**, *50*, 1176–1178.

(6) Ke, W.; Kanatzidis, M. G. Prospects for Low-Toxicity Lead-Free Perovskite Solar Cells. *Nat. Commun.* **2019**, *10*, 965.

(7) Li, S.; Luo, J.; Liu, J.; Tang, J. Self-Trapped Excitons in All-Inorganic Halide Perovskites: Fundamentals, Status, and Potential Applications. *J. Phys. Chem. Lett.* **2019**, *10*, 1999–2007.

(8) Roccanova, R.; Yangui, A.; Nhalil, H.; Shi, H.; Du, M.-H.; Saparov, B. Near-Unity Photoluminescence Quantum Yield in Blue-Emitting Cs 3 Cu 2 Br 5– x I x ($0 \leq x \leq 5$). *ACS Appl. Electron. Mater.* **2019**, *1*, 269–274.

(9) Zhang, R.; Mao, X.; Zheng, D.; Yang, Y.; Yang, S.; Han, K. A Lead-Free All-Inorganic Metal Halide with Near-Unity Green Luminescence. *Laser Photon. Rev.* **2020**, *14*, 2000027.

(10) Pandey, M.; Rasmussen, F. A.; Kuhar, K.; Olsen, T.; Jacobsen, K. W.; Thygesen, K. S. Defect-Tolerant Monolayer Transition Metal Dichalcogenides. *Nano Lett.* **2016**, *16*, 2234–2239.

(11) Jin, H.; Debroye, E.; Keshavarz, M.; Scheblykin, I. G.; Roeffaers, M. B. J.; Hofkens, J.; Steele, J. A. It's a Trap! On the Nature of Localised States and Charge Trapping in Lead Halide Perovskites. *Mater. Horizons* **2020**, *7*, 397–410.

(12) Jun, T.; Sim, K.; Iimura, S.; Sasase, M.; Kamioka, H.; Kim, J.; Hosono, H. Lead-Free Highly Efficient Blue-Emitting Cs 3 Cu 2 I 5 with 0D Electronic Structure. *Adv. Mater.*

2018, *30*, 1804547.

(13) Zeng, F.; Guo, Y.; Hu, W.; Tan, Y.; Zhang, X.; Feng, J.; Tang, X. Opportunity of the Lead-Free All-Inorganic Cs 3 Cu 2 I 5 Perovskite Film for Memristor and Neuromorphic Computing Applications. *ACS Appl. Mater. Interfaces* **2020**, *12*, 23094–23101.

(14) Yuan, D. Air-Stable Bulk Halide Single-Crystal Scintillator Cs 3 Cu 2 I 5 by Melt Growth: Intrinsic and Tl Doped with High Light Yield. *ACS Appl. Mater. Interfaces* **2020**, *12*, 38333–38340.

(15) Kang, J.; Wang, L.-W. High Defect Tolerance in Lead Halide Perovskite CsPbBr3. *J. Phys. Chem. Lett.* **2017**, *8*, 489–493.

(16) Lian, L.; Zheng, M.; Zhang, P.; Zheng, Z.; Du, K.; Lei, W.; Gao, J.; Niu, G.; Zhang, D.; Zhai, T.; et al. Photophysics in Cs 3 Cu 2 X 5 (X = Cl, Br, or I): Highly Luminescent Self-Trapped Excitons from Local Structure Symmetrization. *Chem. Mater.* **2020**, *32*, 3462–3468.

(17) Kresse, G.; Furthmüller, J. Efficient Iterative Schemes for Ab Initio Total-Energy Calculations Using a Plane-Wave Basis Set. *Phys. Rev. B* **1996**, *54*, 11169–11186.

(18) Perdew, J. P.; Burke, K.; Ernzerhof, M. Generalized Gradient Approximation Made Simple. *Phys. Rev. Lett.* **1996**, *77*, 3865–3868.

(19) Kresse, G.; Joubert, D. From Ultrasoft Pseudopotentials to the Projector Augmented-Wave Method. *Phys. Rev. B* **1999**, *59*, 1758–1775.

(20) Monkhorst, H. J.; Pack, J. D. Special Points for Brillouin-Zone Integrations. *Phys. Rev. B* **1976**, *13*, 5188–5192.

(21) Nunes, R. W.; Gonze, X. Berry-Phase Treatment of the Homogeneous Electric Field

Perturbation in Insulators. *Phys. Rev. B* **2001**, *63*, 155107.

(22) Fuchs, F.; Rödl, C.; Schleife, A.; Bechstedt, F. Efficient Approach to Solve the Bethe-Salpeter Equation for Excitonic Bound States. *Phys. Rev. B* **2008**, *78*, 085103.

(23) Lany, S.; Zunger, A. Assessment of Correction Methods for the Band-Gap Problem and for Finite-Size Effects in Supercell Defect Calculations: Case Studies for ZnO and GaAs. *Phys. Rev. B* **2008**, *78*, 235104.

(24) Zhang, S.; Northrup, J. Chemical Potential Dependence of Defect Formation Energies in GaAs: Application to Ga Self-Diffusion. *Phys. Rev. Lett.* **1991**, *67*, 2339–2342.

(25) Liu, N.; Yam, C. First-Principles Study of Intrinsic Defects in Formamidinium Lead Triiodide Perovskite Solar Cell Absorbers. *Phys. Chem. Chem. Phys.* **2018**, *20*, 6800–6804.

(26) Lian, L.; Zheng, M.; Zhang, W.; Yin, L.; Du, X.; Zhang, P.; Zhang, X.; Gao, J.; Zhang, D.; Gao, L.; et al. Efficient and Reabsorption-Free Radioluminescence in Cs 3 Cu 2 I 5 Nanocrystals with Self-Trapped Excitons. *Adv. Sci.* **2020**, *7*, 2000195.

(27) Hull, S.; Berastegui, P. Crystal Structures and Ionic Conductivities of Ternary Derivatives of the Silver and Copper Monohalides—II: Ordered Phases within the (AgX)x–(MX)1−x and (CuX)x–(MX)1−x (M=K, Rb and Cs; X=Cl, Br and I) Systems. *J. Solid State Chem.* **2004**, *177*, 3156–3173.

(28) Heyd, J.; Scuseria, G. E.; Ernzerhof, M. Hybrid Functionals Based on a Screened Coulomb Potential. *J. Chem. Phys.* **2003**, *118*, 8207–8215.

(29) Guo, Z.; Li, J.; Pan, R.; Cheng, J.; Chen, R.; He, T. All-Inorganic Copper (I)-Based Ternary Metal Halides: Promising Materials toward Optoelectronics. *Nanoscale* **2020**.

(30) Li, Y.; Vashishtha, P.; Zhou, Z.; Li, Z.; Shivarudraiah, S. B.; Ma, C.; Liu, J.; Wong, K. S.; Su, H.; Halpert, J. E. Room Temperature Synthesis of Stable, Printable Cs 3 Cu 2 X 5 (X = I, Br/I, Br, Br/Cl, Cl) Colloidal Nanocrystals with Near-Unity Quantum Yield Green Emitters (X = Cl). *Chem. Mater.* **2020**, *32*, 5515–5524.

(31) Protesescu, L.; Yakunin, S.; Bodnarchuk, M. I.; Krieg, F.; Caputo, R.; Hendon, C. H.; Yang, R. X.; Walsh, A.; Kovalenko, M. V. Nanocrystals of Cesium Lead Halide Perovskites (CsPbX 3 , X = Cl, Br, and I): Novel Optoelectronic Materials Showing Bright Emission with Wide Color Gamut. *Nano Lett.* **2015**, *15*, 3692–3696.

(32) Motti, S. G.; Meggiolaro, D.; Martani, S.; Sorrentino, R.; Barker, A. J.; De Angelis, F.; Petrozza, A. Defect Activity in Lead Halide Perovskites. *Adv. Mater.* **2019**, *31*, 1901183.

(33) Wei, S.-H.; Zhang, S. B. Chemical Trends of Defect Formation and Doping Limit in II-VI Semiconductors: The Case of CdTe. *Phys. Rev. B* **2002**, *66*, 155211.

(34) Zhang, S. B.; Wei, S.-H.; Zunger, A. Intrinsic n -Type versus p -Type Doping Asymmetry and the Defect Physics of ZnO. *Phys. Rev. B* **2001**, *63*, 075205.

(35) Jain, A.; Ong, S. P.; Hautier, G.; Chen, W.; Richards, W. D.; Dacek, S.; Cholia, S.; Gunter, D.; Skinner, D.; Ceder, G.; et al. Commentary: The Materials Project: A Materials Genome Approach to Accelerating Materials Innovation. *APL Mater.* **2013**, *1*, 011002.

(36) Stoliaroff, A.; Jobic, S.; Latouche, C. An Ab Initio Perspective on the Key Defects of CsCu 5 Se 3 , a Possible Material for Optoelectronic Applications. *J. Phys. Chem. C* **2020**, *124*, 4363–4368.

(37) Meng, J.; Lan, Z.; Abdellah, M.; Yang, B.; Mossin, S.; Liang, M.; Naumova, M.; Shi, Q.; Gutierrez Alvarez, S. L.; Liu, Y.; et al. Modulating Charge-Carrier Dynamics in Mn-

Doped All-Inorganic Halide Perovskite Quantum Dots through the Doping-Induced Deep Trap States. *J. Phys. Chem. Lett.* **2020**, *11*, 3705–3711.

(38) Huang, Y.; Yin, W.-J.; He, Y. Intrinsic Point Defects in Inorganic Cesium Lead Iodide Perovskite CsPbI 3. *J. Phys. Chem. C* **2018**, *122*, 1345–1350.

(2) Yang, S.; Fu, W.; Zhang, Z.; Chen, H.; Li, C.-Z. Recent Advances in Perovskite Solar Cells: Efficiency, Stability and Lead-Free Perovskite. *J. Mater. Chem. A* **2017**, *5*, 11462–11482.

(3) Sebastia-Luna, P.; Navarro-Alapont, J.; Sessolo, M.; Palazon, F.; Bolink, H. J. Solvent-Free Synthesis and Thin-Film Deposition of Cesium Copper Halides with Bright Blue Photoluminescence. *Chem. Mater.* **2019**, *31*, 10205–10210.

(4) Luo, Z.; Li, Q.; Zhang, L.; Wu, X.; Tan, L.; Zou, C.; Liu, Y.; Quan, Z. 0D $Cs_3Cu_2X_5$ (X = I, Br, and Cl) Nanocrystals: Colloidal Syntheses and Optical Properties. *Small* **2020**, *16*, 1905226.

(5) Jun, T.; Sim, K.; Iimura, S.; Sasase, M.; Kamioka, H.; Kim, J.; Hosono, H. 81-5: Late-News Paper: Pb-free Blue-emitting 0D $Cs_3Cu_2I_5$ with High PLQY of ~90%. *SID Symp. Dig. Tech. Pap.* **2019**, *50*, 1176–1178.

(6) Ke, W.; Kanatzidis, M. G. Prospects for Low-Toxicity Lead-Free Perovskite Solar Cells. *Nat. Commun.* **2019**, *10*, 965.

(7) Li, S.; Luo, J.; Liu, J.; Tang, J. Self-Trapped Excitons in All-Inorganic Halide Perovskites: Fundamentals, Status, and Potential Applications. *J. Phys. Chem. Lett.* **2019**, *10*, 1999–2007.

(8) Roccanova, R.; Yangui, A.; Nhalil, H.; Shi, H.; Du, M.-H.; Saparov, B. Near-Unity Photoluminescence Quantum Yield in Blue-Emitting $Cs_3Cu_2Br_{5-x}I_x$ ($0 \leq x \leq 5$). *ACS Appl. Electron. Mater.* **2019**, *1*, 269–274.

(9) Zhang, R.; Mao, X.; Zheng, D.; Yang, Y.; Yang, S.; Han, K. A Lead-Free All-Inorganic Metal Halide with Near-Unity Green Luminescence. *Laser Photon. Rev.* **2020**, *14*, 2000027.

(10) Pandey, M.; Rasmussen, F. A.; Kuhar, K.; Olsen, T.; Jacobsen, K. W.; Thygesen, K. S. Defect-Tolerant Monolayer Transition Metal Dichalcogenides. *Nano Lett.* **2016**, *16*, 2234–2239.

(11) Jin, H.; Debroye, E.; Keshavarz, M.; Scheblykin, I. G.; Roeffaers, M. B. J.; Hofkens, J.; Steele, J. A. It's a Trap! On the Nature of Localised States and Charge Trapping in Lead Halide Perovskites. *Mater. Horizons* **2020**, *7*, 397–410.

(12) Jun, T.; Sim, K.; Iimura, S.; Sasase, M.; Kamioka, H.; Kim, J.; Hosono, H. Lead-Free Highly Efficient Blue-Emitting $Cs_3Cu_2I_5$ with 0D Electronic Structure. *Adv. Mater.* **2018**, *30*, 1804547.

(13) Zeng, F.; Guo, Y.; Hu, W.; Tan, Y.; Zhang, X.; Feng, J.; Tang, X. Opportunity of the Lead-Free All-Inorganic $Cs_3Cu_2I_5$ Perovskite Film for Memristor and Neuromorphic Computing Applications. *ACS Appl. Mater. Interfaces* **2020**, *12*, 23094–23101.

(14) Yuan, D. Air-Stable Bulk Halide Single-Crystal Scintillator $Cs_3Cu_2I_5$ by Melt Growth: Intrinsic and Tl Doped with High Light Yield. *ACS Appl. Mater. Interfaces* **2020**, *12*, 38333–38340.

(15) Kang, J.; Wang, L.-W. High Defect Tolerance in Lead Halide Perovskite $CsPbBr_3$. *J.*

Phys. Chem. Lett. **2017**, *8*, 489–493.

(16) Lian, L.; Zheng, M.; Zhang, P.; Zheng, Z.; Du, K.; Lei, W.; Gao, J.; Niu, G.; Zhang, D.; Zhai, T.; et al. Photophysics in $Cs_3Cu_2X_5$ (X = Cl, Br, or I): Highly Luminescent Self-Trapped Excitons from Local Structure Symmetrization. *Chem. Mater.* **2020**, *32*, 3462–3468.

(17) Kresse, G.; Furthmüller, J. Efficient Iterative Schemes for Ab Initio Total-Energy Calculations Using a Plane-Wave Basis Set. *Phys. Rev. B* **1996**, *54*, 11169–11186.

(18) Perdew, J. P.; Burke, K.; Ernzerhof, M. Generalized Gradient Approximation Made Simple. *Phys. Rev. Lett.* **1996**, *77*, 3865–3868.

(19) Kresse, G.; Joubert, D. From Ultrasoft Pseudopotentials to the Projector Augmented-Wave Method. *Phys. Rev. B* **1999**, *59*, 1758–1775.

(20) Monkhorst, H. J.; Pack, J. D. Special Points for Brillouin-Zone Integrations. *Phys. Rev. B* **1976**, *13*, 5188–5192.

(21) Nunes, R. W.; Gonze, X. Berry-Phase Treatment of the Homogeneous Electric Field Perturbation in Insulators. *Phys. Rev. B* **2001**, *63*, 155107.

(22) Fuchs, F.; Rödl, C.; Schleife, A.; Bechstedt, F. Efficient O (N_2) Approach to Solve the Bethe-Salpeter Equation for Excitonic Bound States. *Phys. Rev. B* **2008**, *78*, 085103.

(23) Lany, S.; Zunger, A. Assessment of Correction Methods for the Band-Gap Problem and for Finite-Size Effects in Supercell Defect Calculations: Case Studies for ZnO and GaAs. *Phys. Rev. B* **2008**, *78*, 235104.

(24) Zhang, S.; Northrup, J. Chemical Potential Dependence of Defect Formation Energies in GaAs: Application to Ga Self-Diffusion. *Phys. Rev. Lett.* **1991**, *67*, 2339–2342.

(25) Lian, L.; Zheng, M.; Zhang, W.; Yin, L.; Du, X.; Zhang, P.; Zhang, X.; Gao, J.; Zhang, D.; Gao, L.; et al. Efficient and Reabsorption-Free Radioluminescence in $Cs_3Cu_2I_5$ Nanocrystals with Self-Trapped Excitons. *Adv. Sci.* **2020**, *7*, 2000195.

(26) Hull, S.; Berastegui, P. Crystal Structures and Ionic Conductivities of Ternary Derivatives of the Silver and Copper Monohalides—II: Ordered Phases within the $(AgX)_x$–$(MX)_{1-x}$ and $(CuX)_x$–$(MX)_{1-x}$ (M=K, Rb and Cs; X=Cl, Br and I) Systems. *J. Solid State Chem.* **2004**, *177*, 3156–3173.

(27) Guo, Z.; Li, J.; Pan, R.; Cheng, J.; Chen, R.; He, T. All-Inorganic Copper (I)-Based Ternary Metal Halides: Promising Materials toward Optoelectronics. *Nanoscale* **2020**, *12*, 15560-15576.

(28) Li, Y.; Vashishtha, P.; Zhou, Z.; Li, Z.; Shivarudraiah, S. B.; Ma, C.; Liu, J.; Wong, K. S.; Su, H.; Halpert, J. E. Room Temperature Synthesis of Stable, Printable $Cs_3Cu_2X_5$ (X = I, Br/I, Br, Br/Cl, Cl) Colloidal Nanocrystals with Near-Unity Quantum Yield Green Emitters (X = Cl). *Chem. Mater.* **2020**, *32*, 5515–5524.

(29) Protesescu, L.; Yakunin, S.; Bodnarchuk, M. I.; Krieg, F.; Caputo, R.; Hendon, C. H.; Yang, R. X.; Walsh, A.; Kovalenko, M. V. Nanocrystals of Cesium Lead Halide Perovskites ($CsPbX_3$, X = Cl, Br, and I): Novel Optoelectronic Materials Showing Bright Emission with Wide Color Gamut. *Nano Lett.* **2015**, *15*, 3692–3696.

(30) Motti, S. G.; Meggiolaro, D.; Martani, S.; Sorrentino, R.; Barker, A. J.; De Angelis, F.; Petrozza, A. Defect Activity in Lead Halide Perovskites. *Adv. Mater.* **2019**, *31*, 1901183.

(31) Wei, S.-H.; Zhang, S. B. Chemical Trends of Defect Formation and Doping Limit in II-VI Semiconductors: The Case of CdTe. *Phys. Rev. B* **2002**, *66*, 155211.

(32) Zhang, S. B.; Wei, S.-H.; Zunger, A. Intrinsic n -Type versus p -Type Doping Asymmetry and the Defect Physics of ZnO. *Phys. Rev. B* **2001**, *63*, 075205.

(33) Jain, A.; Ong, S. P.; Hautier, G.; Chen, W.; Richards, W. D.; Dacek, S.; Cholia, S.; Gunter, D.; Skinner, D.; Ceder, G.; et al. Commentary: The Materials Project: A Materials Genome Approach to Accelerating Materials Innovation. *APL Mater.* **2013**, *1*, 011002.

(34) Stoliaroff, A.; Jobic, S.; Latouche, C. An Ab Initio Perspective on the Key Defects of $CsCu_5Se_3$, a Possible Material for Optoelectronic Applications. *J. Phys. Chem. C* **2020**, *124*, 4363–4368.

(35) Meng, J.; Lan, Z.; Abdellah, M.; Yang, B.; Mossin, S.; Liang, M.; Naumova, M.; Shi, Q.; Gutierrez Alvarez, S. L.; Liu, Y.; et al. Modulating Charge-Carrier Dynamics in Mn-Doped All-Inorganic Halide Perovskite Quantum Dots through the Doping-Induced Deep Trap States. *J. Phys. Chem. Lett.* **2020**, *11*, 3705–3711.

(36) Huang, Y.; Yin, W.-J.; He, Y. Intrinsic Point Defects in Inorganic Cesium Lead Iodide Perovskite $CsPbI_3$. *J. Phys. Chem. C* **2018**, *122*, 1345–1350.

TOC Graphic

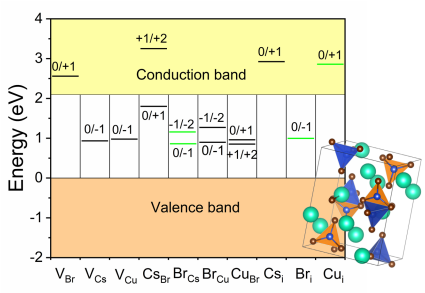
Energy (eV)
Conduction band
Valence band
+1/+2
0/+1
0/+1
0/+1
0/-1
0/-1
0/+1
-1/-2
0/-1
-1/-2
0/+1
+1/+2
0/-1
V_{Br} V_{Cs} V_{Cu} Cs_{Br} Br_{Cs} Br_{Cu} Cu_{Br} Cs_i Br_i Cu_i